JAERI-Research
94-033

ANALYSIS OF HIGH ENERGY ION RIPPLE LOSS IN THE UP-DOWN ASYMMETRIC CONFIGURATION BY OFMC PLUS MAPPING HYBRID CODE

November 1994

Sergei KONOVALOV*, Tomonori TAKIZUKA, Keiji TANI
Kiyotaka HAMAMATSU and Masafumi AZUMI

日本原子力研究所
Japan Atomic Energy Research Institute

本レポートは，日本原子力研究所が不定期に公刊している研究報告書です。

入手の問合わせは，日本原子力研究所技術情報部情報資料課（〒319-11 茨城県那珂郡東海村）あて，お申し越しください。なお，このほかに財団法人原子力弘済会資料センター（〒319-11 茨城県那珂郡東海村日本原子力研究所内）で複写による実費頒布をおこなっております。

This report is issued irregularly.

Inquiries about availability of the reports should be addressed to Information Division, Department of Technical Information, Japan Atomic Energy Research Institute, Tokai-mura, Naka-gun, Ibaraki-ken 319-11, Japan.

編集兼発行　日本原子力研究所
印　　刷　いばらき印刷㈱

JAERI-Research 94-033

Analysis of High Energy Ion Ripple Loss in the Up-down Asymmetric Configuration by OFMC Plus Mapping Hybrid Code

Sergei KONOVALOV*, Tomonori TAKIZUKA, Keiji TANI
Kiyotaka HAMAMATSU and Masafumi AZUMI

Department of Fusion Plasma Research
Naka Fusion Research Establishment
Japan Atomic Energy Research Institute
Naka-machi, Naka-gun, Ibaraki-ken

(Received October 11, 1994)

New version of a Mapping code for the up-down asymmetric configuration is developed. Combination of Mapping with OFMC, a Hybrid code, provides an effective tool for reliable and fast calculations of high energy ion ripple losses in a tokamak including both total loss fraction and lost power distribution over the first wall. Results of the analysis by this Hybrid code on the NBI ion ripple losses in JT-60U are in a good agreement with experimental and previous OFMC data.

Keywords: Tokamak, Up-down Asymmetry, Ripple, Ripple Loss, High Energy Ion, Alpha Particle, ITER, NBI, JT-60U, OFMC Code, Mapping Code, Hybrid Code

---

* I.V. Kurchatov Institute of Atomic Energy, Moscow, Russia

ＯＦＭＣとマッピングの混成コードによる上下非対称配位中の高エネルギー・イオン・リップル損失の解析

日本原子力研究所那珂研究所炉心プラズマ研究部
Sergei KONOVALOV*・滝塚　知典・谷　　啓二
濱松　清隆・安積　正史

（1994年10月11日受理）

上下非対称配位に対する新しいマッピングコードを開発した、マッピングとＯＦＭＣを組み合わせた混成コードは、トカマクにおける高エネルギーイオンのリップル損失の計算を、リップル損失割合のみならず第一壁への損失パワー分布についても、正確にかつ速く行う。ＪＴ－60Ｕにおける ＮＢＩイオンのリップル損失に対する混成コードによる解析結果は、実験結果及びこれまでのＯＦＭＣ計算結果に良く一致した。

那珂研究所：〒311－01　茨城県那珂郡那珂町大字向山801-1
* クルチャトフ研究所

Contents

目　　次

1. Introduction

Ripple losses of fusion α particles and associated heat load on the tokamak first wall and in-vessel components are considered to be one of the major limitations on fusion reactor design. The evaluation of ripple losses of the suprathermal ions is a traditional problem in a tokamak study and has a long history. The physics of ripple effects on the fast ion confinement in main is well understood. It made possible to employ simplified numerical algorithms for fast estimation of total loss fraction based on kinetic [1,2,3] or mapping [4,5] approach. However distribution of the heat load over a tokamak first wall can not be obtained with this codes. Traditionally last problem was studied by means of the time consuming Orbit Following Monte-Carlo (OFMC) codes [6] or with combination of the mapping and OFMC [2].

Nowadays the single null equilibrium configuration is considered to be the most favorable for future tokamak fusion reactors. Due to the top-bottom asymmetry of this configuration, ripple amplitudes in up and down reflection points of a banana orbit are different. It leads to the additional transport mechanism [7,8] primarily considered in association with ripple assistant heating/fueling of a tokamak plasma by perpendicularly injected neutral beam [7,9]. In a vertically asymmetric configuration banana particles with reflection points within ripple well region undergo net radial drift [7,8]. The origin of this drift is that the local magnetic field maxima shield banana trajectories from some region of reflection phase. In result, the ripple induced radial displacement of a banana tip, which is averaged over the reflection phase, differs from zero [10]. Then if up and down banana reflection points have different ripple amplitude the difference in mean values of vertical displacement at these points defines the velocity of the net banana drift. The direction of this drift is always opposite to direction of the $[\nabla \mathbf{B} \times \mathbf{B}]$ ion drift.

The transport processes for particles with reflection points inside the ripple well region were examined in [8]. It was found that in the high collisionality regime the diffusion of toroidaly trapped particles, associated with vertical asymmetry is compensated by the additional diffusive flux of the locally trapped particles and resulting diffusive transport turns out to be exactly the same as in the vertically symmetric case. At low collisions, e.g. for high energy ions, when the ion drift is codirected with gradient of the ripple amplitude, particles with reflection points in the ripple well region are trapped into local wells and escape to the first wall. If the ion drift is reversed, the trapping probability decreases, while the net outward drift expels banana particles out of the plasma. It means that the ripple well region can be considered as an instant loss cone for both ion drift directions. Therefore, if the top-bottom asymmetry affects the ripple induced transport in the local well region only,

one should expect no difference in the total loss fraction when the toroidal field direction is reversed. However in the recent OFMC calculations of the α particle ripple losses in ITER, essential difference in the power loss fractions between for up and down ion-drift directions was found [11]. The origin of this difference should be examined. In the present work, we didn't treat this problem but developed a new code to solve this problem.

A new Mapping code to study ripple losses of the suprathermal ions in a tokamak with up-down asymmetric equilibrium has been developed. A Hybrid code has also been developed, which is the combination of the Mapping with OFMC calculations. The Mapping is applied outside the ripple well region, and the OFMC is inside and in the vicinity of the ripple well region. This code provides reasonable data on the total loss fraction as well as on the distribution of the lost power over the first wall at least 10 times faster than a pure OFMC code. In section 2 brief description of the OFMC part of the Hybrid code is presented. Section 3 is devoted to the Mapping formulation, it's features and applicability region. In section 4 combination of the Mapping and OFMC parts into the Hybrid code is presented. Results of the benchmark calculation of the ripple losses of NBI ions in JT-60 are given in section 5. Derivation of the Monte-Carlo collisional operators for the OFMC and the Mapping is outlined in Appendix.

2. OFMC

In the Orbit Following part of a Hybrid code, the standard set of drift motion equations is solved:

$$\frac{d\mathbf{r}}{dt} = V\chi\frac{\mathbf{B}}{B} + \frac{\rho_{L0}V^2(1+\chi^2)}{2V_0B^2}[\mathbf{B}\times\nabla\mathbf{B}], \qquad (1)$$

where $\chi = V_{//}/V$ is a cosine of pitch angle, $\rho_{L0} = \rho_{L0}(V_0, B)$ is a Larmor radius at initial velocity V_0. [**E** x **B**] drift for suprathermal ions is considered much smaller than gradient and curvature ones and is excluded from calculations at present. As it was shown in [12, 13] electrical drift doesn't affect total ripple loss fraction of NBI ions in JT-60U but causes the shift in the peak position of heat wall load due to losses of the ripple trapped particles and also leads to a small (within 10%) redistribution of ripple losses between banana and locally trapped channels. For fusion alphas one can expect such effects only for fully slowed-down particles. The term proportional to [**B** x rot **B**] is also omitted due to the standard tokamak condition of low beta value.

The axisymmetric field is represented in the form:

$$\mathbf{B} = \frac{1}{R}\mathbf{e}_\varphi + \frac{1}{R}[\nabla\Psi\times\mathbf{e}_\varphi]. \qquad (2)$$

one should expect no difference in the total loss fraction when the toroidal field direction is reversed. However in the recent OFMC calculations of the α particle ripple losses in ITER, essential difference in the power loss fractions between for up and down ion-drift directions was found [11]. The origin of this difference should be examined. In the present work, we didn't treat this problem but developed a new code to solve this problem.

A new Mapping code to study ripple losses of the suprathermal ions in a tokamak with up-down asymmetric equilibrium has been developed. A Hybrid code has also been developed, which is the combination of the Mapping with OFMC calculations. The Mapping is applied outside the ripple well region, and the OFMC is inside and in the vicinity of the ripple well region. This code provides reasonable data on the total loss fraction as well as on the distribution of the lost power over the first wall at least 10 times faster than a pure OFMC code. In section 2 brief description of the OFMC part of the Hybrid code is presented. Section 3 is devoted to the Mapping formulation, it's features and applicability region. In section 4 combination of the Mapping and OFMC parts into the Hybrid code is presented. Results of the benchmark calculation of the ripple losses of NBI ions in JT-60 are given in section 5. Derivation of the Monte-Carlo collisional operators for the OFMC and the Mapping is outlined in Appendix.

2. OFMC

In the Orbit Following part of a Hybrid code, the standard set of drift motion equations is solved:

$$\frac{d\mathbf{r}}{dt} = V\chi\frac{\mathbf{B}}{B} + \frac{\rho_{L0}V^2(1+\chi^2)}{2V_0B^2}[\mathbf{B}\times\nabla\mathbf{B}], \qquad (1)$$

where $\chi = V_{//}/V$ is a cosine of pitch angle, $\rho_{L0} = \rho_{L0}(V_0, B)$ is a Larmor radius at initial velocity V_0. [**E** x **B**] drift for suprathermal ions is considered much smaller than gradient and curvature ones and is excluded from calculations at present. As it was shown in [12, 13] electrical drift doesn't affect total ripple loss fraction of NBI ions in JT-60U but causes the shift in the peak position of heat wall load due to losses of the ripple trapped particles and also leads to a small (within 10%) redistribution of ripple losses between banana and locally trapped channels. For fusion alphas one can expect such effects only for fully slowed-down particles. The term proportional to [**B** x rot **B**] is also omitted due to the standard tokamak condition of low beta value.

The axisymmetric field is represented in the form:

$$\mathbf{B} = \frac{1}{R}\mathbf{e}_\varphi + \frac{1}{R}[\nabla\Psi\times\mathbf{e}_\varphi]. \qquad (2)$$

Here and henceforth the following normalized quantities are used: R, Z are normalized by R_{ax} (a major radius of the magnetic axis), velocity by the initial value V_0, magnetic field components by the vacuum toroidal field at the magnetic axis $B_{\varphi 0}(R_{ax})$, poloidal flux Ψ is normalized by $2\pi R_{ax}^2 B_{\varphi 0}(R_{ax})$. The para- or diamagnetism in B_φ is neglected at present because of its little effect on the ripple loss.

To take into account the ripple we add a single harmonic perturbation

$$B_\varphi^{ripple} = \frac{1}{R}\delta(R, Z)\cos N\varphi \ , \qquad (3)$$

to the toroidal field component only, because of it's dominant effect [14]. Here N is the number of the toroidal field coil sections. Note that resulting non divergence free field can be used for particle orbit analysis in drift motion approach in contrast to full equation where non divergent field leads to distortion of magnetic moment. In this case all components of perturbation field should be taken into account.

In the axisymmetric case, equation (1) preserves the toroidal momentum, which can be written in the form

$$\Psi_b = \rho_{L0} R V \chi \frac{B_\varphi}{B} + \Psi(R, Z) \ . \qquad (4)$$

Without collisional scattering the ratio of magnetic moment to particle energy remains constant during slowing down. This nondimensional magnetic moment,

$$\nu = \frac{\mu}{E} = \frac{1 - \chi^2}{B} \ , \qquad (5)$$

altogether with the toroidal momentum in form (4) have a clear geometric sense ($\nu \approx R_{reflection}$) and can be employed for mapping construction.

In the Orbt Following part, equation (1) is solved using fourth order Runge-Kutta algorithm with automatic time step control based on conservation of invariant ν (5). Additional restriction on the time step value originates from the necessity to provide "sufficient" number of steps at every spatial period of the perturbation. For the ripple loss problem the latest restriction is dominant. Two-dimensional cubic splines are used for poloidal flux and ripple amplitude to provide smooth interpolation of the magnetic field together with necessary derivatives. Changes in pitch and energy values due to collisions are generated by a Monte-Carlo technique (see Appendix) at every time step. Cylindrical (R, φ, Z) spatial coordinates are used for easy incorporation of a tokamak constructive elements of arbitrary geometry into calculations.

3. Mapping

3.1 Formulation of mapping

Since the dominant deviation of Ψ_b from axisymmetric value is accumulated in the vicinity of the turning point, the drift motion equations can be reduced to a map with time step $\Delta t = \tau_b/2$. It is important to choose appropriate grid variables for the map. We use a coordinate system (ρ, λ, φ); ρ is the radial grid coordinate on a magnetic surface and φ is the toroidal angle. Instead of the poloidal angle for up-down asymmetric equilibria it is convenient to introduce a new variable,

$$\lambda = \mathrm{sign}(I_p B_R) \frac{\nu - \nu_{max}(\rho)}{\nu_{min}(\rho) - \nu_{max}(\rho)} \quad . \tag{6}$$

The value of λ ranges from -1 to 1 and always positive above mid plane ($B_R = 0$ surface). Then successive up and down reflection points in axisymmetric field correspond to $(\rho, \pm\lambda)$ points in the mapping variables. Figure 1(a) shows the mapping coordinate for a JT-60U configuration. The applicable region for the mapping in this configuration is limited as shown in the figure, which will be described in sub-section 3.2.

Far from the ripple well region, where $\alpha_* = B_R / \delta N B_\varphi > 1$, the expression for a radial kick takes a simple form:

$$\Delta\rho = \frac{\partial\rho}{\partial\Psi} \mathrm{sign}(B_\varphi)\, \Delta\Psi_b \sin\left(N\varphi + \mathrm{sign}(B_R B_\varphi) \frac{\pi}{4} \right) , \tag{7}$$

where

$$\Delta\Psi_b = \rho_{L0}\, R V \delta \sqrt{\pi N B_\varphi / B_R}\, \frac{\alpha_*^{3/2}}{1 + \alpha_*^{3/2}} \quad . \tag{8}$$

All variables in the last expression are given in above mentioned nondimensional units. Multiplier $\alpha_*^{3/2} / (1 + \alpha_*^{3/2})$ is included to avoid unphysical divergence in the kick amplitude at the ripple well boundary [15]. Sign terms in the first formula provide right dependence of the radial kick on ripple phase for both up and down reflection points and for arbitrary direction of toroidal field (gradient drift) and plasma current I_p.

We employ for calculations an implicit mapping scheme, similar to that of [4];

$$\begin{aligned} \rho_{n+1} &= \rho_n + V \Delta\rho_0 (\rho_{n+1}, \lambda_{n+1}, \varphi_n) \ , \\ \varphi_{n+1} &= \varphi_n + V \Delta_p\varphi_0 (\rho_{n+1}, \lambda_{n+1}) \pm \Delta_1\varphi (\rho_{n+1}, \lambda_{n+1}) + \delta\varphi (\rho_{n+1}, \lambda_{n+1}) \ . \end{aligned} \tag{9}$$

The time steps n, n+1, ... correspond to the turning points as illustrated in Fig. 2. In the last formula $\Delta_1\varphi$ is a phase increment due to the motion along magnetic field line. The toroidal displacement of the reflection point owing to banana precession $\Delta_p\varphi$ is a linear function of the particle velocity. Then $\Delta_p\varphi_0$ and radial displacement amplitude $\Delta\rho_0$ can be precalculated at initial velocity V_0 . The area preserving term $\delta\varphi$ for proposed scheme with $\Delta\rho$ defined by (7) takes the form

$$\delta\varphi = \frac{1}{N}\frac{\partial\Delta\rho}{\partial\rho}\cos\left(N\varphi + \mathrm{sign}(B_R B_\varphi)\frac{\pi}{4}\right) . \qquad (10)$$

Because of $\lambda = \lambda(\rho, \nu)$, the derivative $\partial/\partial\rho = (\partial/\partial\rho)_{\lambda=\mathrm{const}} + (\partial\lambda/\partial\rho)\cdot(\partial/\partial\lambda)_{\rho=\mathrm{const}}$. The radial displacement is evaluated on a surface $\nu = \mathrm{const}$.

In the Mapping code, phase increments $\Delta_p\varphi$ and $\Delta_1\varphi$ as well as necessary bounce averaged coefficients for collisions are given at the mapping grid points beforehand by the Orbit Following calculation . For the radial kick amplitude we take analytical formula (8). Two-dimensional cubic spline interpolation is used for all above mentioned values. The implicit equation for ρ is solved by Newton method. Setting of ρ_n as initial point and smooth spline function for $\Delta\rho$ provide fast convergence of iterations. Collisional corrections to (ρ, ν, V) variables are generated by Monte-Carlo methods (see Appendix) after every bounce period.

3.2 Mapping features and validity region

The mapping applicability region is quite obviously limited by the prompt orbit-loss boundary, which in most cases can be replaced by $\rho = \mathrm{const} \approx 1$ surface, and the ripple well boundary $\alpha_* = 1$ because the particle trapping into the local wells isn't accounted in the mapping. Also one should exclude from the mapping calculation the neighborhood of the inside midplane ($B_R = 0$ surface for $R > R_{ax}$) because the bounce period for barely trapped particles with banana tip in this region become very long. An example of the mapping applicability region for a JT-60U configuration is shown in Fig. 1(a), where the curves of $\alpha_* = 1$ and $\alpha_* = 5$ are drawn.

In the vicinity of the ripple well region with moderate α_* values of $5 \geq \alpha_* \geq 1$, the simple sine dependence of the radial kick on the ripple phase (eq. (7)) is violated. Moreover for a typical tokamak condition in the vicinity of the ripple well boundary, the ripple amplitude δ and therefore the radial displacement amplitude are relatively high. For fusion alphas in this area, ΔZ_b is of order several centimeters and the ripple amplitude δ, owing to steepness of it's profile, varies significantly on the vertical kick length. It leads to a difference in vertical excursion amplitude when direction of the toroidal field and consequently the ion drift is reversed.

Figure 3 shows the displacement of the toroidal momentum Ψ_b versus toroidal phase evaluated by the Orbit Following calculation. We calculated the displacement of fusion alpha particles with birth energy at different values of α_* and for up and down directed ion drift. An ITER EDA equilibrium and ripple data [16] were used in these calculations. To evaluate excursion value, alpha particle orbits were followed backward in time in the axisymmetric field from reflection point $\chi = 0$ with the same poloidal position (R, Z) and successive values of toroidal phase $N\varphi$ up to the intersection of the midplane (actually up to the first point after the intersection where $\cos(N\varphi) = 0$). Then ripple was "switched on" and orbits were calculated forward in time till the next intersection. Figure 4 illustrates the method to evaluate the radial displacement, $(\Psi_b - \Psi_{b0})/\Delta\Psi_b$, near the reflection point. The displacement value is defined as difference between averaged values of Ψ_b (straight segments in Fig. 4) after and before a reflection point.

One can see from Fig. 3(a) that for $\alpha_* > 3$ analytic formula (7) (dotted curve) is in a reasonable agreement with numerical results (solid curve). When the banana tip approaches the ripple well boundary ($\alpha_* \sim 1$), the difference in the maximum displacement amplitude for up (co-directed with $\nabla\delta$) and down (counter-directed with $\nabla\delta$) ion drift is growing along with essential deviation from sine dependence (Fig. 3(b) and (c)). When the ripple value is uniform, this difference vanished and resulting dependence was found to be very similar to analytical one [10]. In a usual tokamak device, there exists the gradient of ripple amplitude $\nabla\delta$, which also affects ripple trapping process. For the case of $\alpha_* \approx 1$ and upward drift (co-directed with $\nabla\delta$), the break of the solid curve in the left of Fig. 3(c) represents the particle trapping into the local well. For reversed drift direction, the trapping into local wells doesn't take place even at lower $\alpha_* \leq 0.5$ value. Therefore, taken into account above mentioned effects, one should shift mapping validity boundary to some moderate value of $\alpha_* \approx 2 \div 4$ from $\alpha_* \approx 1$.

It is important to note that variation of the ripple amplitude and background plasma parameters on a suprathermal ion orbit also limits validity of the mapping application. Especially it relates to analysis of the ripple losses of the charged fusion products in discharges with low field and/or plasma current. In such case the trapped particle orbit has rather a potato than a banana shape and difference in the ripple amplitude at inner and outer part of an orbit can reach $1 \div 3$ order of magnitude and the effect of ripple can't be reduced to local kicks near reflection points. By another words we should apply the present Mapping for simulation of a particle orbit with moderate banana width $\Delta_b << a$, where a is a plasma minor radius.

The ripple perturbation of a tokamak magnetic field results in the formation of drift islands. Spatial location of the islands is determined by the resonance condition

$\Delta_p\varphi = 2\pi k/N$, where k is an integer. The width of the resonance can be estimated as $\Delta_{isl} \approx \sqrt{\Delta Z_b / (\partial \Delta_p\varphi / \partial Z_b)}$. Therefore suprathermal ion dynamics in a rippled field is very sensitive to the details of the spatial profiles of toroidal precession frequency as well as ripple amplitude. Poincare maps for successive banana tip position calculated by (a) the Orbit Following code and (b) the Mapping code are shown in Fig. 5. Increment in the toroidal phase due to banana precession is scaled as $\Delta_p\varphi \propto Vq^2$, where q is the safety factor. Then to get more illustrative figure we used for these calculation an ITER equilibrium with twice as lower current ($q(0.95) \approx 6$) and 5 times artificially increased ripple amplitude. All particle orbits were started from banana tips with the same $R = 7.5$ m , $\varphi = 0$ but different vertical position Z. Ripple wells at these graphs are located above $Z = 5.35$ m. Figure 5(c) shows $2\pi\Delta_p\varphi/N$ versus Z. One can see that positions of the drift islands in Orbit Following and Mapping calculations are similar and coincide with resonance values of the precession frequency (Fig. 5(c)).

It looks very attractive and intuitively valuable to employ an explicit scheme instead of the implicit one (eq. (9)) and therefore to avoid time consuming iterations. The main difficulty for explicit mapping is to deal with distortion of the area preserving. In previous works [4,5] the necessity of including of the area preserving term $\delta\varphi$ in expression for phase increment was examined. In calculations of ripple losses of fast ions as well as in location of the boundary of the ergodic region for many cases, no difference was found in using mapping with or without area preserving correction especially when collisions were accounted. However, in previous cases, the ripple losses of fast ions were studied for tokamaks with high ripple and relatively low plasma current, and considerable part of plasma column was covered by the stochastic region. Total ripple losses of suprathermal ions in such conditions are defined mostly by the width of ergodic region and the effect of area preserving was hardly seen. In the present day tokamak projects with high plasma current and as low as possible ripple amplitude, the stochastic boundary is almost coincide with the ripple well boundary [16]. In such conditions area preserving features of a mapping can drastically affect calculation results.

To study the effect of the area preserving we prepare two simplified variants of the mapping in addition to reference one (eq. (9)). We shall call Mapping 2 the explicit scheme which is the same as eq. (9) except for $\delta\varphi = 0$ and $\Delta\rho = \Delta\rho(\rho_n, \lambda_n)$, and Mapping 3 the explicit mapping where the displacement amplitude is constant within a grid cell and varies from cell to cell. Therefore Mapping 2 doesn't preserve phase volume while distortion of area preserving in Mapping 3 takes place when a banana tip position is moved from cell to cell by a kick.

Figure 6 shows an area preserving features of the different mapping schemes. In upper row, Poincare plots for first 200 bounces are shown. Case (a) corresponds to the reference Mapping (9), (b) to the Mapping 2 and (c) to the Mapping 3. Lower row represents the same pictures but for 200 bounces followed by previous 10000. For alpha particles in ITER, 10000 bounces correspond to approximately 0.05 - 0.1 of the slowing down time τ_S. One can see that the reference Mapping manifested perfect area preserving (Upper ergodic orbits leaves grid area during first 200 bounces and therefore they are not presented at the lower picture). Strong downward drift in the non-area-preserving Mapping 2 affects significantly the calculation results in case of narrow stochastic region and/or low collisions. Mapping 3 shows very similar behavior as reference one, except for region with high ripple amplitude where the drift island width is comparable to or exceeds the grid step size. The lower figure of 6(c) shows that distortion of the area preserving leads to formation an "empty" zone above $Z = 5$ m. This zone could prevent particles to be lost from inner plasma regions.

All 3 mappings use 2D cubic spline interpolation for the toroidal precession frequency because of it's primary importance for correspondence of phase portrait in the Mapping and Orbit Following calculations. Then the gain in CPU time when the reference Mapping is replaced by simplest one (Mapping 3) is not so significant and doesn't exceed 3 times. Because the total CPU time in the Hybrid code expenses in the main deal with calculations with it's Orbit Following part, we employ the reference scheme (9) in this code to avoid additional restrictions on it's applicability. The reference Mapping spends 1s of CPU time for 5000 bounces on the IBM power workstation.

In the present Mapping, collisional operator takes into account not only scattering along magnetic surface as it was done in the previous works [2,4,5] but neoclassical diffusion also. Benchmark calculations for collisional spreading of the delta function particle source revealed fairly good agreement between OFMC and Mapping simulations. Figure 7 shows an example of the time evolution of the second moments, $S_{RR} \equiv \langle (R-\langle R\rangle)^2\rangle$, $S_{RZ} \equiv \langle (R-\langle R\rangle)(Z-\langle Z\rangle)\rangle$ and $S_{ZZ} \equiv \langle (Z-\langle Z\rangle)^2\rangle$, in (a) OFMC and (b) Mapping calculations. The example corresponds to alpha particles with energy 3.52MeV in ITER EDA. Initial point is $R_0 = 8$ m, $Z_0 = 4$ m with $T_e = T_i = 15$ keV, $n_e = 2.17 \times 10^{14}$ cm^{-3}. The bounce time of a banana α particle is $\tau_{b0} = 3.84 \times 10^{-5}$ s.

4. Hybrid code

In the Hybrid code any orbit calculation starts with OFMC part. At every reflection point (if any) applicability of the Mapping is checked and the calculation is switched to the Mapping whenever it is possible. In the same way orbit following is switched back to OFMC if the banana tip leaves from the Mapping validity region (see Fig. 1(a)). For evaluation of new (R, Z) coordinates corresponded to last (ρ, λ), Newton iterations are used. We employ enhancement factor for collisions for passing particles or exclude them from calculations assuming their perfect confinement. The Mapping calculation is at least 50 times faster than OFMC. In the Hybrid code total gain in CPU time depends on the position of the boundary limited mapping application and usually is of factor 10÷30 in comparison with pure OFMC code.

5. Benchmark calculation of the NBI ion ripple losses in JT-60U

Benchmark calculations of ripple losses of NBI ions in JT60-U were carried out to verify new Hybrid code. Previous OFMC and experimental data [12] were used for comparison. Calculation parameters are summarized in Table 1. Ripple contours are shown in Fig. 1(b). Quasi-perpendicular D^0 beams with energy $E_b = 90$ keV were injected. The power fraction of the NBI source is $P(E_b) : P(E_b/2) : P(E_b/3) = 0.78 : 0.15 : 0.07$. The initial position, energy and pitch-angle of a beam ion were generated by Monte-Carlo method according to experimental conditions. Ionization cross-section due to ion and electron impacts was taken from works [17, 18].

Calculation results are summarized in Table 2. Here for comparison previous results of OFMC calculations and experiments [12] are also shown. It is seen that new Hybrid code provides a very similar results to pure OFMC calculations. In Fig. 8 two dimensional distribution of power loss over the first wall is shown, where (a) the present Hybrid code data is compared with (b) the previous OFMC data and (c) experimental data [12]. The poloidal position number on the first wall is plotted at a closed circle in Fig. 1(b). As it was shown in [12], the shift of the hot spot in calculated and experimental data relates to the [**E** x **B**] drift. Energy spectrums of lost particles are given by Fig. 9. The bottom solid line corresponds to ripple trapped losses, and dotted one to banana losses. The upper thick line is the sum of both loss channels. Spectrums and distribution of the heat load obtained with the Hybrid code agree well with previous OFMC data.

4. Hybrid code

In the Hybrid code any orbit calculation starts with OFMC part. At every reflection point (if any) applicability of the Mapping is checked and the calculation is switched to the Mapping whenever it is possible. In the same way orbit following is switched back to OFMC if the banana tip leaves from the Mapping validity region (see Fig. 1(a)). For evaluation of new (R, Z) coordinates corresponded to last (ρ, λ), Newton iterations are used. We employ enhancement factor for collisions for passing particles or exclude them from calculations assuming their perfect confinement. The Mapping calculation is at least 50 times faster than OFMC. In the Hybrid code total gain in CPU time depends on the position of the boundary limited mapping application and usually is of factor 10÷30 in comparison with pure OFMC code.

5. Benchmark calculation of the NBI ion ripple losses in JT-60U

Benchmark calculations of ripple losses of NBI ions in JT60-U were carried out to verify new Hybrid code. Previous OFMC and experimental data [12] were used for comparison. Calculation parameters are summarized in Table 1. Ripple contours are shown in Fig. 1(b). Quasi-perpendicular D^0 beams with energy $E_b = 90$ keV were injected. The power fraction of the NBI source is $P(E_b) : P(E_b/2) : P(E_b/3) = 0.78 : 0.15 : 0.07$. The initial position, energy and pitch-angle of a beam ion were generated by Monte-Carlo method according to experimental conditions. Ionization cross-section due to ion and electron impacts was taken from works [17, 18].

Calculation results are summarized in Table 2. Here for comparison previous results of OFMC calculations and experiments [12] are also shown. It is seen that new Hybrid code provides a very similar results to pure OFMC calculations. In Fig. 8 two dimensional distribution of power loss over the first wall is shown, where (a) the present Hybrid code data is compared with (b) the previous OFMC data and (c) experimental data [12]. The poloidal position number on the first wall is plotted at a closed circle in Fig. 1(b). As it was shown in [12], the shift of the hot spot in calculated and experimental data relates to the [**E** x **B**] drift. Energy spectrums of lost particles are given by Fig. 9. The bottom solid line corresponds to ripple trapped losses, and dotted one to banana losses. The upper thick line is the sum of both loss channels. Spectrums and distribution of the heat load obtained with the Hybrid code agree well with previous OFMC data.

6. Summary

A new Mapping code to study ripple effects on the suprathermal ion confinement in a tokamak with up-down asymmetric equilibrium has been developed.

Poincare maps obtained in the Mapping and Orbit Following calculations indicate that present Mapping scheme gives adequate description of noncollisional ion dynamics in a rippled magnetic field.

Bounce averaged collisional operator taking into account neoclassical diffusion term extends the mapping applicability region. Comparison of the Mapping results on Coulomb scattering and energy diffusion processes were found to be in a good agreement with those of the OFMC code for ions in a wide energy range from $1.5\,T_i$ to 4 MeV.

A Hybrid code has been developed, which combines the Mapping with OFMC calculations , and gives 10÷30 times faster calculation than a pure OFMC code.

Benchmarking of the new code against previous OFMC and experimental data for ripple losses of NBI ions in JT-60U showed that the Hybrid code provides reliable results as for the total power loss fraction as well as for the distribution of the heat load over the first wall.

Acknowledgments

Valuable discussion with Dr. S. Putvinski and his assistance in derivation of the mapping collisional operator are gratefully acknowledged.

One of the authors (SK) is indebted to the JAERI for hospitality and financial support during a visit under the JAERI foreign researcher inviting program.

6. Summary

A new Mapping code to study ripple effects on the suprathermal ion confinement in a tokamak with up-down asymmetric equilibrium has been developed.

Poincare maps obtained in the Mapping and Orbit Following calculations indicate that present Mapping scheme gives adequate description of noncollisional ion dynamics in a rippled magnetic field.

Bounce averaged collisional operator taking into account neoclassical diffusion term extends the mapping applicability region. Comparison of the Mapping results on Coulomb scattering and energy diffusion processes were found to be in a good agreement with those of the OFMC code for ions in a wide energy range from $1.5\,T_i$ to 4 MeV.

A Hybrid code has been developed, which combines the Mapping with OFMC calculations , and gives 10÷30 times faster calculation than a pure OFMC code.

Benchmarking of the new code against previous OFMC and experimental data for ripple losses of NBI ions in JT-60U showed that the Hybrid code provides reliable results as for the total power loss fraction as well as for the distribution of the heat load over the first wall.

Acknowledgments

Valuable discussion with Dr. S. Putvinski and his assistance in derivation of the mapping collisional operator are gratefully acknowledged.

One of the authors (SK) is indebted to the JAERI for hospitality and financial support during a visit under the JAERI foreign researcher inviting program.

References

[1] F.S. Zaitsev, A.P. Smirnov, P.N. Yushmanov, Nucl. Fusion **26** (1986) 1311.

[2] G. Kamelander, S. Konovalov, S. Putvinski, V. Saplahidy, A. Smirnov, in Plasma Physics and Controlled Nuclear Fusion Research 1990 (Proc. 13th Int. Conf., Washington, D.C.,1990), Vol. 3, IAEA, Vienna, (1991) 533.

[3] S.V. Putvinskiet al, JET-P(93)68, submitted to Nucl. Fusion.

[4] R.B. White, A.H. Boozer, R.J. Goldston, R. Hay, J. Albert, C.F.F. Karney, in Plasma Physics and Controlled Nuclear Fusion Research 1982 (Proc. 9th Int. Conf., Baltimore, 1982), Vol. 3, IAEA, Vienna (1983) 391.

[5] J.J. Foit, K. Tani, T.Takizuka, M. Azumi, JAERI-M 88-249 (1988).

[6] K. Tani, T. Takizuka, M. Azumi, Nucl. Fusion **23** (1983) 657.

[7] R.J. Goldston, D.L. Jassby, PPPL report MATT-1244 (1976).

[8] P.N. Yushmanov, J.R. Cary, S.G. Shaharina, Nucl. Fusion **33** (1993) 1293.

[9] K. Tani, R. Yoshino, T. Tuda, T. Takizuka, M. Azumi, Fusion Technology **21** (1992) 103.

[10] R.J. Goldston, H.H. Towner, J. Plasma Phys. **26** (1981) 283.

[11] K. Tani, "Ripple Losses of Alpha Particles in ITER," to be published in JAERI-Research.

[12] K. Tani, K. Tobita, T. Neyatani, H. Takeuchi, T. Tuda, M. Azumi, Proc. of IAEA Technical Committee Meeting on Alpha Particles in Fusion Research, Trieste, 1993, IAEA, Vienna (1993) 67.

[13] T. Nishitani, K. Tobita, K. Tani et al., Plasma Physics and Controlled Nuclear Fusion Research 1992, (Proc.14th Int. Conf., Wurzburg, 1992), Vol. 1, IAEA, Vienna, (1993) 351.

[14] P.N. Yushmanov, in Rew. of Plasma Physics, Vol. 16, Consultant Bureau, New York, (1990) 117.

[15] L.M. Kovrizhnykh, Nucl. Fusion **24** (1984) 851.

[16] ITER JCT, "Detail of the ITER Outline Design Report," TAC-4, San-Diego, Jan. 1994 (1994).

[17] R.K. Janev, C.D. Boley, D.E. Post, Nucl. Fusion **29** (1989) 2125.

[18] D.L. Galbraith, T. Kammash, Nucl. Fusion **19** (1979) 1047.

Table 1 Calculation parameters for NBI ion ripple losses in JT-60U

toroidal magnetic field	B_t = 4.1 T at R=3.22m
plasma current	I_p = 4.0 MA
plasma temperature	$T_e(\Psi) = T_{e0}[(1-\gamma_e)(1-\Psi^{1.7})^{0.7}+\gamma_e]$
	T_{e0} = 2.74 keV
	γ_e = 0.02
	$T_i(\Psi) = T_{i0}[(1-\gamma_i)(1-\Psi^{1.3})^{0.8}+\gamma_i]$
	T_{i0} = 4.1 keV
	γ_i = 0.02
plasma density	$n_e(\Psi) = n_{e0}[(1-\gamma_n)(1-\Psi^{1.3})^{0.75}+\gamma_n]$
	$n_{e0} = 5.3 \times 10^{19}$ m^{-3}
	γ_n = 0.02
effective Z	Z_{eff} = 2.5 (uniform)
charge number of impurity	Z_{imp} = 8 (oxygen)
number of TF coils	N = 18

Table 2 Comparison of the Hybrid code and OFMC data

Particle Loss

particle loss fractions (%)	Hybrid code	OFMC
banana drift losses	18.27	18.69
ripple trapped losses	10.38	9.92
total losses	28.65	28.61

Power Loss

power loss fractions (%)	Hybrid code	OFMC
banana drift losses	15.56	15.9
ripple trapped losses	8.73	8.0
total losses	24.29	23.9

Experimental result for the ripple trapped power loss fraction is 8.3 ± 1.4%

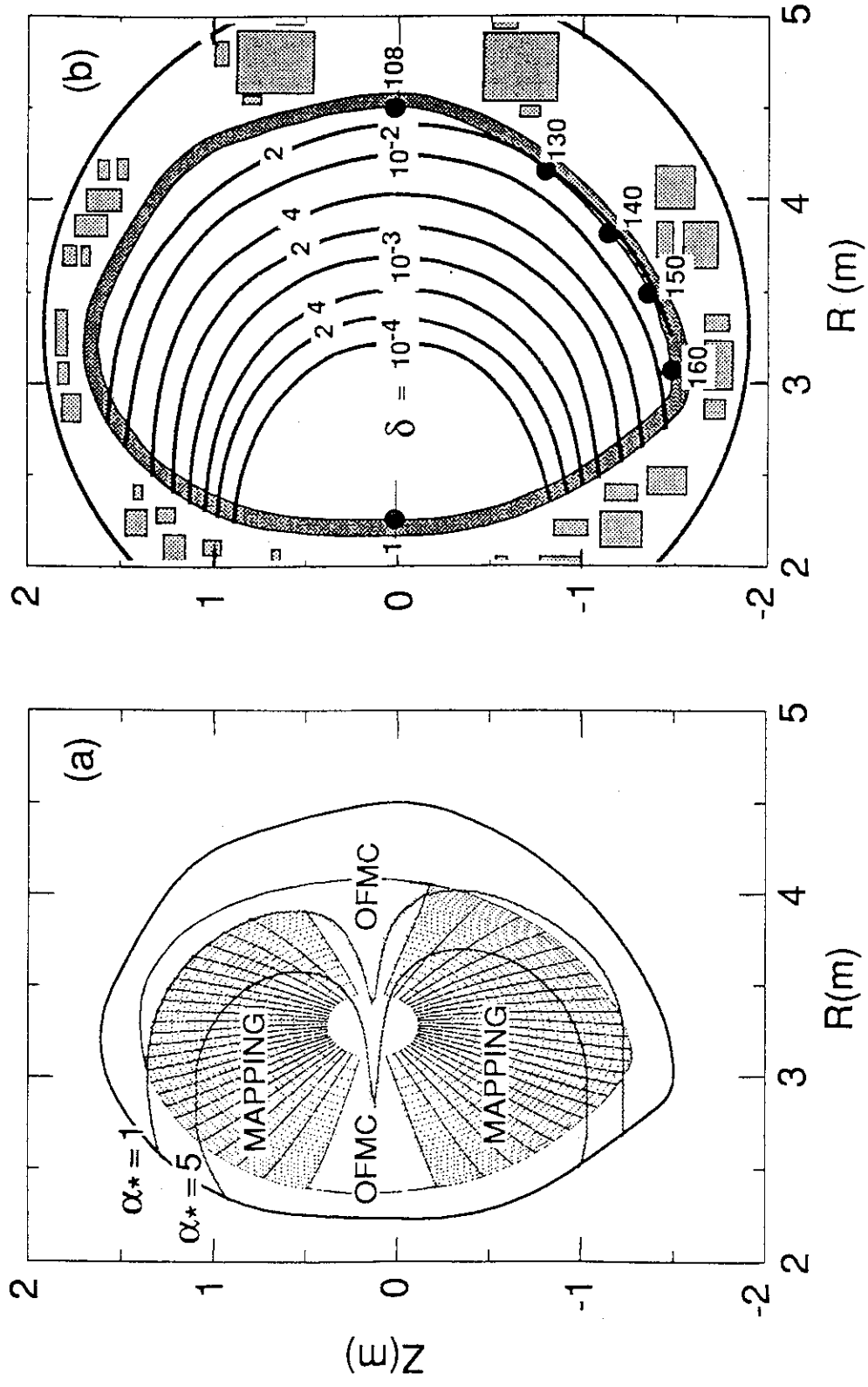

Fig. 1 Mapping coordinate system and validity region in a JT-60U configuration. The curves of α^*=1 and of α^*=5 are also drawn in (a). Figure (b) shows the ripple contours. The poloidal position number on the first wall is plotted at a closed circle.

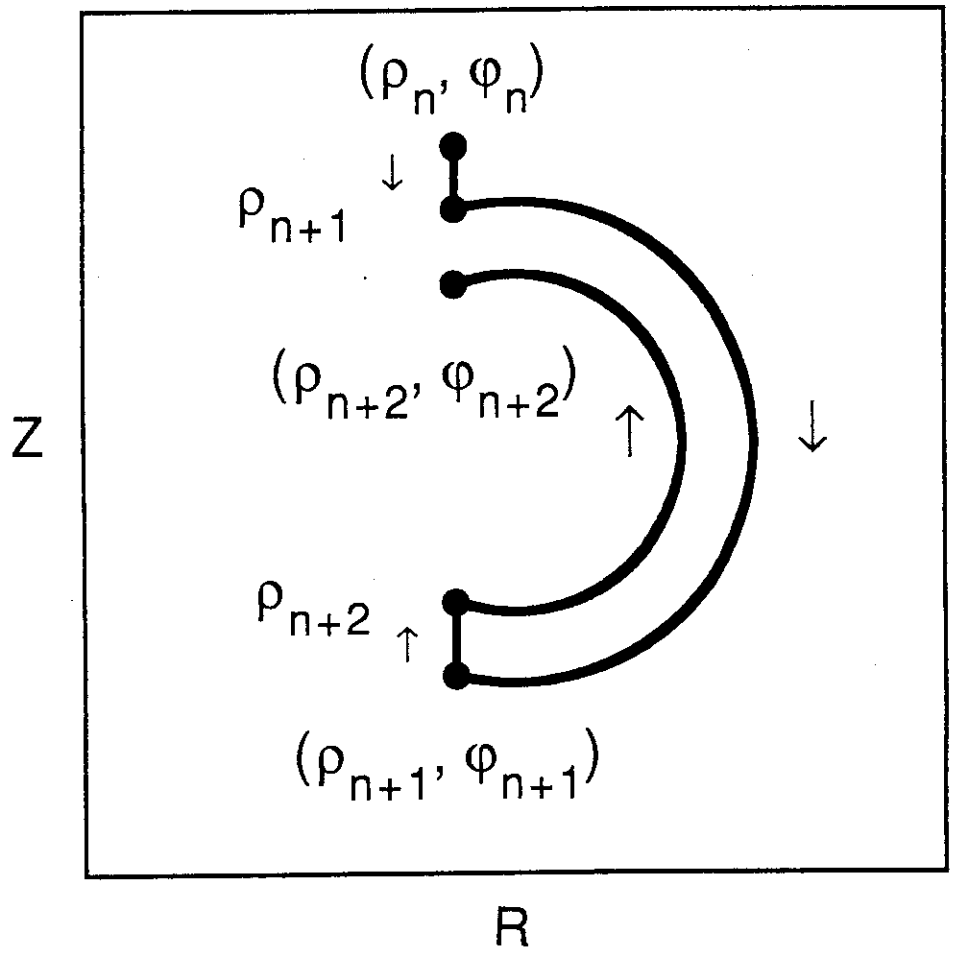

Fig. 2 Time steps of the Mapping for turning points of a banana particle in a tokamak with toroidal field ripple.

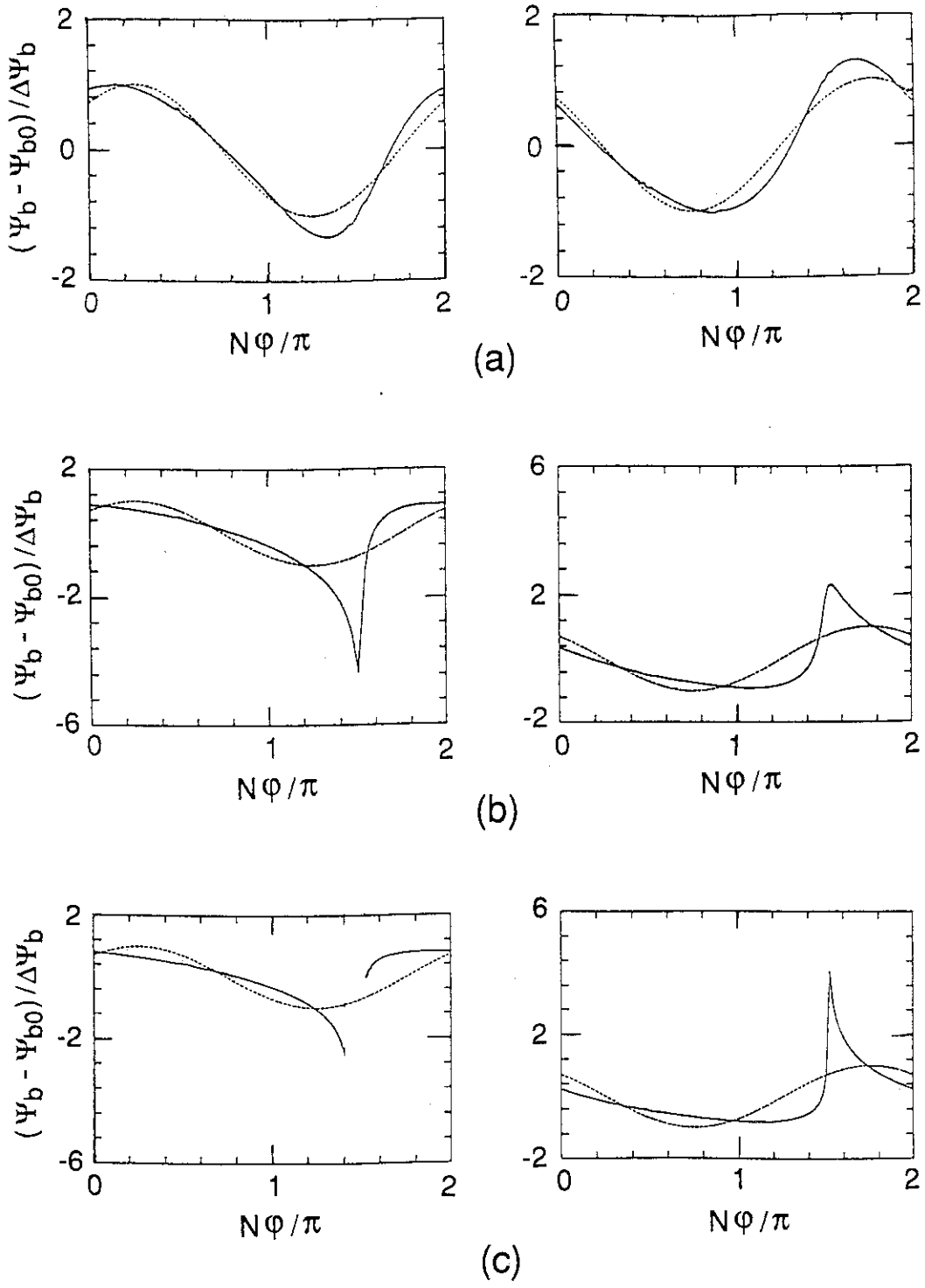

Fig. 3 Dependence of ripple produced radial displacement on the reflection phase evaluated by the Orbit Following calculation. The displacement of the toroidal momentum Ψ_b is normalized by $\Delta\Psi_b$ given by eq. (8). Initial points of α particles in ITER for the Orbit Following calculation were taken at the same major radius R=9.5 m, and for different value of Z: (a) Z=4.0 m, α*=3.52, (b) Z=4.64 m, α*=1.34, and (c) Z=4.8 m, α*=1.01. Left figures correspond to upward (co-directed with $\nabla\delta$) ion drift, and right to downward (counter-directed with $\nabla\delta$) ion drift. The brake of the solid curve in the left of (c) represents the particle trapping into the local well.

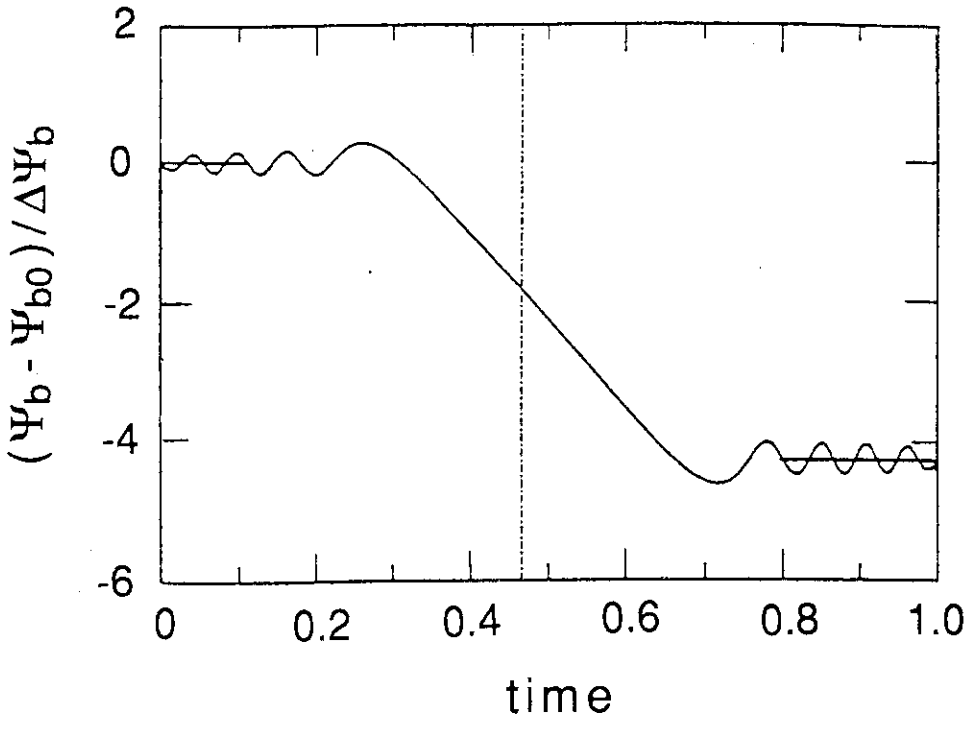

Fig. 4 Toroidal momentum Ψ_b versus time along banana orbit. Vertical dotted line corresponds to the reflection point. Radial displacement value is defined as difference between averaged values (straight segments) of Ψ_b after and before the reflection.

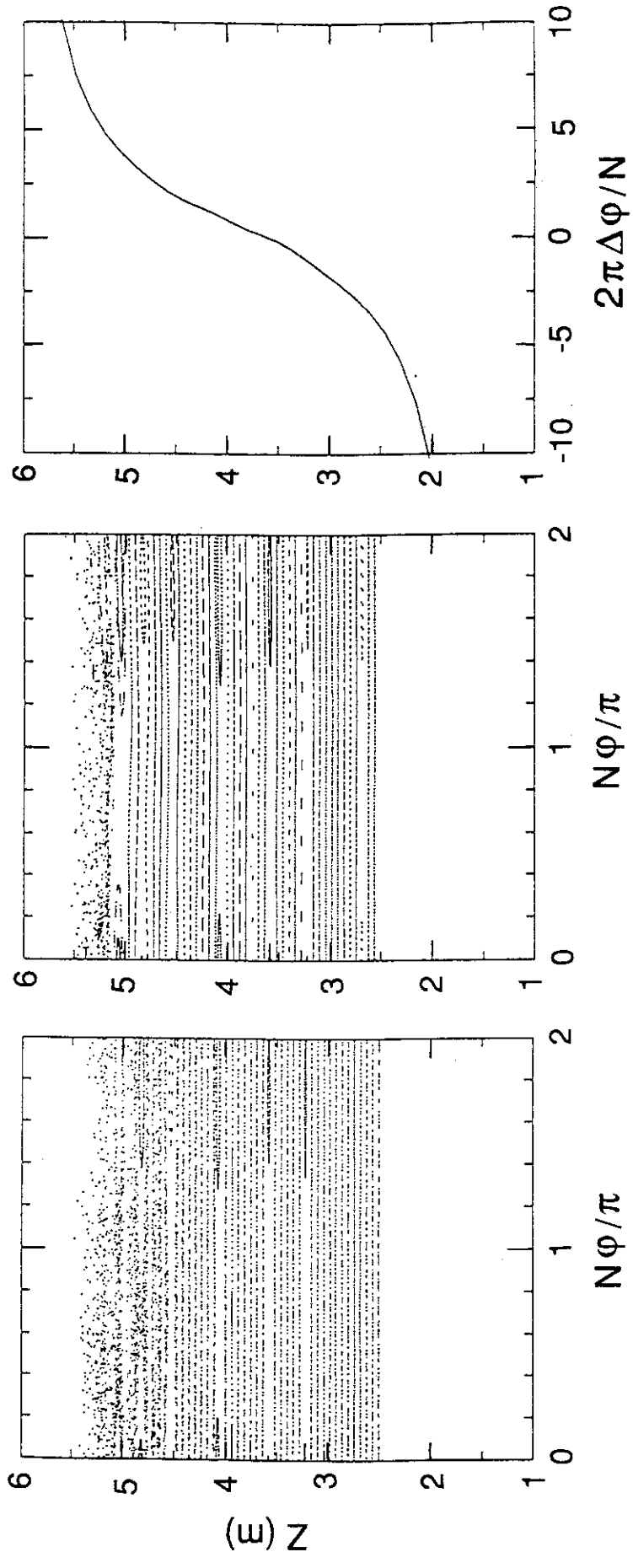

Fig.5 Poincare map for successive banana tip positions from (a) OFMC and (b) Mapping calculations. Phase increment due to banana toroidal precession versus Z is shown in (c) which points out the resonance positions. Initial positions of banana tips of α particles are R=7.5 m, φ=0, and various Z values in ITER.

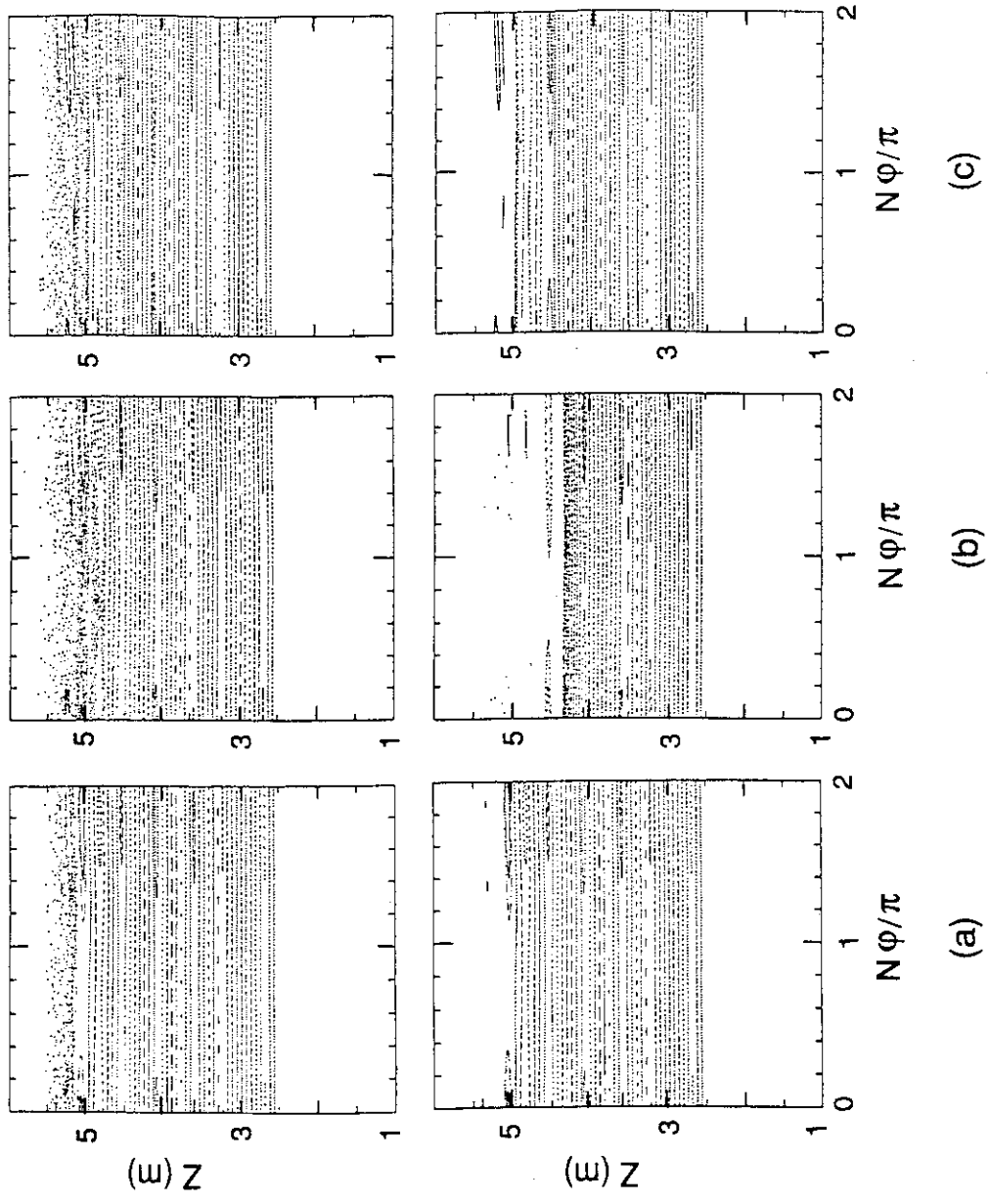

Fig. 6 Area preserving feature of the different Mapping scheme. Upper row pictures correspond to trajectories at their first 200 bounce periods. Lower row shows the same orbits but 10000 bounces latter. Case (a) corresponds to the reference Mapping, (b) to the Mapping 2 and (c) to the Mapping 3. Parameters are the same as those in Fig. 5.

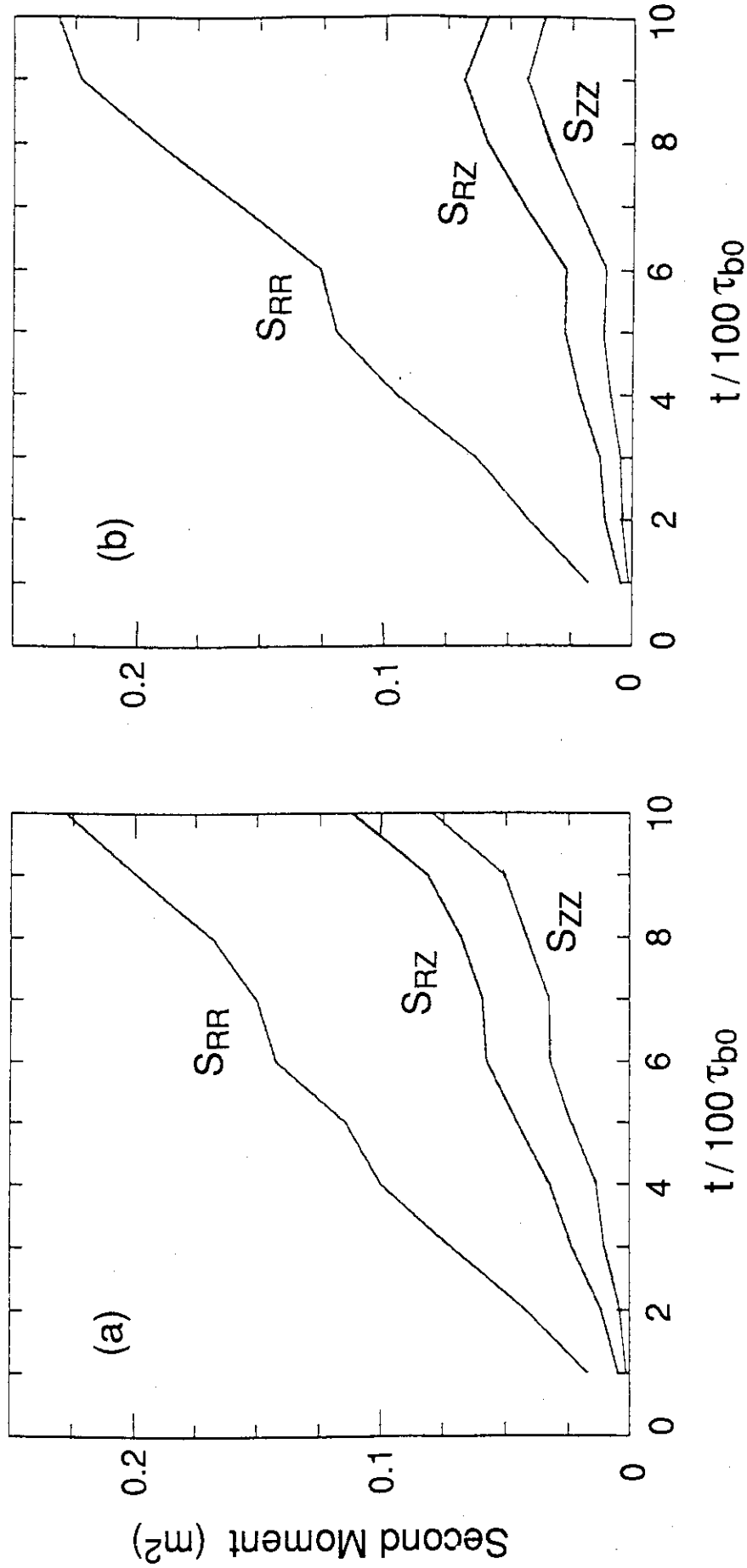

Fig. 7 Comparison of pitch angle scattering in (a) OFMC and (b) Mapping calculations. Curves correspond to the second moments S_{RR}, S_{RZ}, and S_{ZZ} from top to bottom.

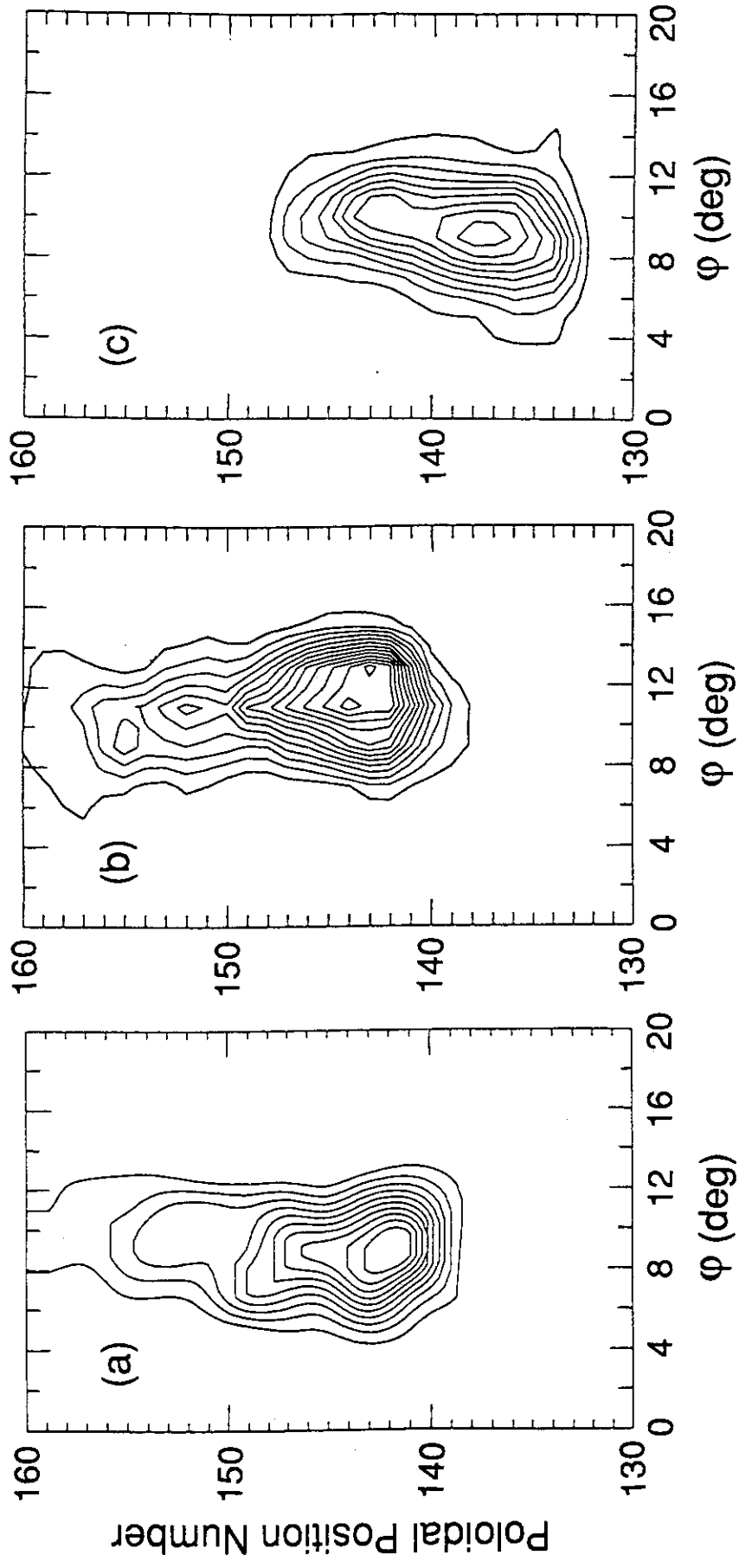

Fig. 8 Two-dimensional distribution of the lost power over the first wall for NBI heating in JT-60U. Figure (a) is the result of the Hybrid code calculations, (b) is that of OFMC calculations and (c) is experimental result. Equi-contours are drawn with the interval of 0.03 MW/m².

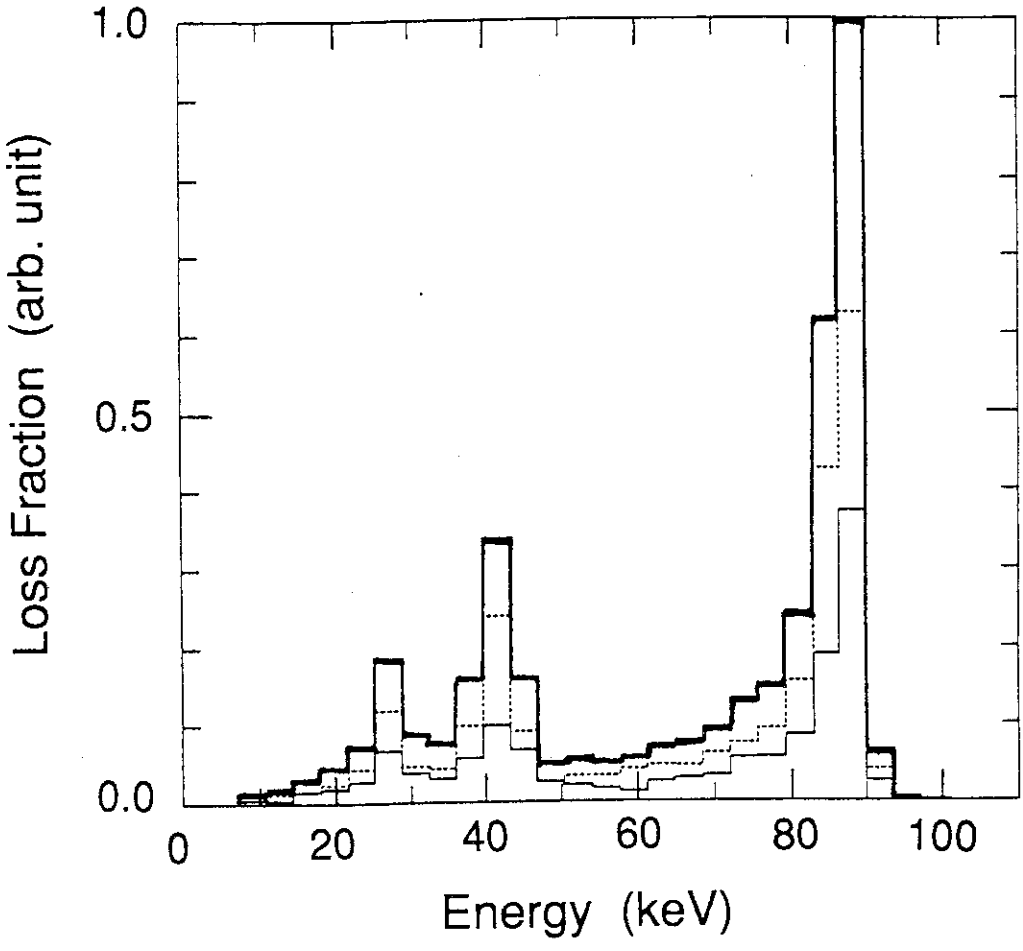

Fig. 9 Energy spectrums of the lost particles. Bottom solid line corresponds to ripple trapped losses, dotted one to banana losses, and upper thick line is the total loss spectrum.

Appendix Monte-Carlo collisional operators

Collisional term in the drift kinetic equation can be represented as

$$\frac{df}{dt} = \frac{1}{\tau_s}\{\frac{V_c^3}{V^2}\frac{\partial}{\partial V}[A(V)f + V B(V)\frac{\partial f}{\partial V}] + D(V)\frac{\partial}{\partial \chi}(1-\chi^2)\frac{\partial f}{\partial \chi}\} \quad , \qquad (A1)$$

where the first term related to the slowing down and energy diffusion and second one to the pitch angle scattering of fast ions by the background plasma species. Here

$$\tau_s = 3 m T_e^{3/2} (4\sqrt{2\pi m_e}\, n_e Z^2 e^4 \lambda_e)^{-1} = 0.02 \frac{10}{\lambda_e}\frac{m}{m_e}\frac{1}{Z^2}\frac{(T_e\,keV)^{3/2}}{n_e/10^{14}}$$

is a slowing down time (second), where m is the fast ion mass, m_e the electron mass and λ the Coulomb logarism. In the slowing down and energy diffusion term, both background electron and ion impacts are taken into account:

$$A(V) = a_i(u) + \frac{V^3}{V_c^3} \quad ,$$

$$B(V) = \frac{T_i}{2E_0}\frac{1}{V^2}\left(a_i(u) + \frac{T_e}{T_i}\frac{V^3}{V_c^3}\right) \quad ,$$

where u is a ratio of the fast ion velocity to the background ion thermal velocity

$$u = V\frac{V_0}{V_i} \quad .$$

For pitch angle scattering we keep ion contribution only;

$$D(V) = \frac{V_b^3}{V^3}\, u\, C_i(u) \quad .$$

For Maxwellian plasma, coefficients depending on relative velocity can be represented as follows

$$a_i(u) = Erf(u) - \frac{2}{\sqrt{\pi}}\, u \exp(-u^2) \quad ,$$

$$C_i(u) = \frac{1}{4}\left(\frac{2}{u} - \frac{1}{u^3}\right) Erf(u) + \frac{1}{2\sqrt{\pi}}\frac{\exp(-u^2)}{u^2} \quad .$$

At velocity V_c power transfer from fast ions to electrons is equal to that to bulk plasma ions

$$V_c = \frac{1}{V_0}\left[\frac{3\sqrt{\pi}}{4}\frac{m_e\lambda_i}{\lambda_e}\sum_j\frac{n_j Z_j^2}{n_e m_j}\right]^{1/3}\left[\frac{2T_e}{m_e}\right]^{1/2},$$

where index j is referred to plasma ion species. The similar coefficient for pitch angle scattering takes the form

$$V_b = \frac{1}{V_0}\left[\frac{3\sqrt{\pi}}{4}\frac{m_e\lambda_i}{m\lambda_e}Z_{eff}\right]^{1/3}\left[\frac{2T_e}{m_e}\right]^{1/2},$$

where the effective charge number is given as

$$Z_{eff} = \sum\frac{n_j Z_j^2}{n_e}.$$

Usually, when the loss of fusion α particles is studied, the asymptotic values for scattering coefficients are used. At $u >> 1$, one can get $a_j(u) = 1$, $B(V) = 0$, $D(V) = 0.5\,(V_b/V)^3$. However for NBI ions with initial energy of order 70 - 100 keV, the energy and pitch angle diffusion rates are approximately 100 times higher than those for alphas in spite of the slowing down time can be of the same order of magnitude. Then in our code we employ most general expression for diffusion coefficients.

We derive the Monte-Carlo equivalent of the operator (A1) following to [i] by evaluating first and second central moments for velocity and pitch angle. In result we have the recurrent formulas;

$$\chi_{n+1} = \chi_n\left(1 - 2D(V)\frac{\Delta t}{\tau_s}\right) + \xi_\chi\sqrt{2D(V)\left(1-\chi_n^2\right)\frac{\Delta t}{\tau_s}}, \qquad (A2)$$

$$V_{n+1} = V_n + \frac{\Delta t}{\tau_s}\frac{V_c^3}{V^2}\left[-A(V) + \frac{\partial}{\partial V}\left(V B(V)\right)\right] + \xi_V\sqrt{2B(V)\frac{V_c^3}{V}\frac{\Delta t}{\tau_s}}, \qquad (A3)$$

where Δt is a time step value, ξ is a Gaussian random number with zero mean and unit dispersion. As it was shown in [i], the Gaussian random number can be replaced by ± 1 random number with equal probability for plus and minus. Using of Gaussian random number, however, makes possible to increase time step value, and it is employed to the present mapping scheme.

To derive the scattering operator for the Mapping, one should average (A1) over a bounce period; $\Delta t = \tau_b$. We shall assume that the variation of the bulk plasma

---

[i] A.H. Boozer, G. Kuo-Petravic, Phys. Fluids **24** (1981) 851.

parameters such as densities and temperatures for all species can be neglected on a banana width scale. This assumption is quite appropriate for NBI ions in JT-60U as well as for fusion α-s in ITER and matches with general limits of present Mapping scheme. Then the bounce-averaged energy diffusion operator for the Mapping is exactly the same as eq. (A3).

We transform the pitch angle scattering term in (A1) to axisymmetric COM variables and after averaging over bounce period we obtain

$$\frac{\partial f}{\partial t} = \frac{1}{\tau_b}\frac{\partial}{\partial C_i}\tau_b < A^{ik} > \frac{\partial f}{\partial C_k} \quad , \tag{A4}$$

$$A^{ik} = \frac{D(V)}{\tau_s}(1-\chi^2)\frac{\partial C_i}{\partial \chi}\frac{\partial C_k}{\partial \chi} \quad , \tag{A5}$$

$$<\cdots> = \frac{1}{\tau_b}\int_0^{\tau_b}\cdots dt \quad ,$$

where $C_1 = \rho$, $C_2 = \nu$ and τ_b is a bounce period. Evaluating first and second central momentums for ρ and ν one can get Monte-Carlo equivalent for (A4) :

$$\nu_{n+1} = \nu_n + \frac{\Delta t}{\tau_s}\left[\frac{\partial}{\partial \nu}(\tau_b < A^{\nu\nu} >) + \frac{\partial}{\partial \rho}(\tau_b < A^{\nu\rho} >)\right] + \xi_\nu \sqrt{2 < A^{\nu\nu} > \Delta t} \quad , \tag{A6}$$

$$\rho_{n+1} = \rho_n + \frac{\Delta t}{\tau_s}\left[\frac{\partial}{\partial \rho}(\tau_b < A^{\rho\rho} >) + \frac{\partial}{\partial \nu}(\tau_b < A^{\nu\rho} >)\right] + \xi_\nu \sqrt{\frac{2\Delta t}{< A^{\rho\rho} >}} < A^{\nu\rho} >$$
$$+ \xi_\rho \sqrt{\frac{2\Delta t}{< A^{\nu\nu} >}} \sqrt{< A^{\nu\nu} >< A^{\rho\rho} > - < A^{\nu\rho} >^2} \quad . \tag{A7}$$

Using the same assumptions as for energy diffusion operator, we can remove all profile dependent variables out of the integral sign and represent diffusion coefficients in (A6) and (A7) as follows;

$$\tau_b < A^{\rho\rho} > = \frac{D(V)}{\tau_s}\left\{\rho_{L0} V \left(\frac{\partial \rho}{\partial \Psi}\right)\right\}^2 \int_0^{\tau_b} dt\,(1-\chi^2)\left(\frac{RB_\varphi}{B}\right)^2 \quad ,$$

$$\tau_b < A^{\nu\rho} > = \frac{D(V)}{\tau_s}\rho_{L0} V \left(\frac{\partial \rho}{\partial \Psi}\right)\int_0^{\tau_b} dt\,(1-\chi^2)\left(-\frac{2R\chi\, B_\varphi}{B^2}\right) \quad , \tag{A8}$$

$$\tau_b < A^{\nu\nu} > = \frac{4D(V)}{\tau_s}\int_0^{\tau_b} dt\,\frac{\chi^2(1-\chi^2)}{B^2} \quad .$$

All coefficients A^{ij} in (A8) can be written with multiplier τ_b. Since $\Delta t / \tau_b = 1$, it allows to exclude time from the Mapping calculation if stationary problem is considered.

Usually neoclassical terms in (A6) and (A7) are omitted due to more than order of magnitude difference in diffusion rates along and across magnetic surfaces and only A^{vv} term was taken into account. In most cases such approach doesn't affect much the total power loss fraction. However the distribution of lost power over the first wall, especially due to losses of ripple trapped particles, is very sensitive to the ripple-enhanced collisional outward flux over the ripple well boundary. Therefore the neoclassical terms should be employed in calculations for evaluation of the heat load.

Note that all integrals in (A8) can be represented in the form $I^{ij}(V) = g(V)\, I^{ij}(V_0)$. For coefficients $A^{\rho\rho}$ and A^{vv} we have $g(V) = 1/V$ according to $\tau_b \sim 1/V$. For the cross term $A^{v\rho}$, we have $g(V) = 1$, because a trpped particle changes its sign of χ during a bounce time and $I^{v\rho}(V) = \int_0^{\tau_b} dt\, F\chi \sim \frac{dF}{d\rho}\, \rho_{banana}\, \tau_b \sim V^0$ ($\rho_{banana} \sim V$ is the banana width). We checked these scalings numerically and have got fairly good agreement for all energy range from ~10 keV (beam ions) to ~5 MeV (alphas). It makes it possible to avoid 3D interpolations for scattering coefficients.

Then finally we use in the Mapping calculation operators (A3), (A6) and (A7), where all coefficients are precalculated at initial energy at the grid points. Two-dimensional cubic spline interpolations for spatial variables and explicit dependencies on energy are used for the evaluation of the coefficients at any point (ρ, λ, V).